Real-Time Assessment of Spatial and Temporal Coupled Catalysis within Polyelectrolyte Microcapsules Containing Coimmobilized Glucose Oxidase and Peroxidase

Erich W. Stein,[†,‡] Dmitry V. Volodkin,[†] Michael J. McShane,*[,‡] and Gleb B. Sukhorukov[†,§]

Max-Planck Institute of Colloids and Interfaces, Golm/Potsdam, 14476, Germany, and Institute of Micromanufacturing, Louisiana Tech University, Ruston, Louisiana 71272

Received May 1, 2005; Revised Manuscript Received January 6, 2006

The encapsulation of biological enzymes within polyelectrolyte microcapsules is an important step toward microscale devices for processing and analytical applications, one which could be applied to the realization of minimally invasive sensing technology. In this work, the encapsulation and functional characterization of a bienzymatic coupled catalytic system within polyelectrolyte microcapsules is described. The two components, glucose oxidase (GOx) and horseradish peroxidase (HRP), were coprecipitated with calcium carbonate microspheres, followed by layer-by-layer assembly to form ultrathin polymer film coatings that act as capsule walls after removal of the sacrificial carbonate cores. Encapsulated concentrations of GOx and HRP were determined to be 19.7 ± 1.0 and 29.4 ± 3.6 mg/mL, respectively. An 85% decrease in the rate of glucose consumption relative to GOx and HRP in free solution was observed, which is attributed to substrate diffusion limitations. To further understand the temporal and spatial dynamics of the two-step reaction, a technique for monitoring microscale glucose consumption was developed using confocal imaging techniques. Time-based acquisition of capsule/Amplex Red suspensions was performed, from which it was observed that the high concentration of enzyme immobilized within the capsule walls resulted in a greater rate and quantity of glucose consumption at the capsule periphery when compared to glucose consumption within the capsule interior. These findings demonstrate the function of a bienzymatic catalytic system within the controlled environment of polyelectrolyte microspheres and a novel approach to analysis of the internal reactions using confocal imaging that will allow direct comparison with reaction−diffusion modeling and further explorations to optimize the distribution and activity of the encapsulated species.

Introduction

The ability to sequester molecules within a controlled volume or compartment is of considerable interest to the design of biological sensors, in particular, protein-based sensors comprising components that may be cytotoxic and/or immunogenic.[1] By compartmentalizing the sensing chemistry within a semipermeable capsule, allowing transport of the analyte of interest across the compartment barrier, the molecular recognition and specific interaction with the analyte can occur without compromising the surrounding environment. Microscale carriers offer easy introduction into to the sample of interest, via injection or infusion.[2,3] While traditional methods of localizing sensing components include component immobilization within hydrogel,[4] silica,[5] and polymer[6] matrixes, recent developments using carriers fabricated by nanoassembly techniques offer promise for biological sensing applications.[7−12] In particular, developments involving enzyme immobilization within mesoporous particles,[13] precipitated crystals,[11] enzyme-doped ultrathin films,[14,15] and calcium alginate microspheres in combination with self-assembled multilayers[16,17] provide several immobilization options from which to select.

Layer-by-layer (LbL) self-assembly, a technique based on the adsorption of charged molecules or particles onto an oppositely charged substrate,[18] has been demonstrated for preparation of ultrathin films with precisely controlled properties such as thickness, composition, and permeability.[15,19−22] Additionally, methods to simply and efficiently produce polymeric capsules have been developed utilizing this technique through LbL film deposition of charged polyelectrolytes onto sacrificial templates, which are subsequently dissolved.[23] Recently, microcapsule fabrication has transitioned from polymer templates (e.g., melamine formaldehyde) to inorganic particles, such as manganese, cadmium, and calcium carbonate microparticles,[24] which can be dissolved with mild core dissolution conditions that favor complete template dissolution and retention of enzymatic activity.[24,25] Whereas traditional encapsulation methods based on techniques involving alterations of pH [26,27] and solvent polarity [23] along with initial-layer decomplexation [28] have been shown to encapsulate molecules, exposure to harsh conditions can reduce biological viability of the molecules, which could potentially limiting these methods for enzymatic-based sensor fabrication.

An additional advantage of calcium carbonate ($CaCO_3$) particles is the characteristic mesoporous structure, such that, during LbL film deposition, polyelectrolyte complexes adsorb not only to the particle surface but also within the interpenetrating pores. Following core dissolution, a polyelectrolyte capsule containing a polyelectrolyte matrix that spans the capsule interior remains.[29] Three methods of macromolecular encapsulation have been previously demonstrated using polyelectrolyte microcapsules fabricated from $CaCO_3$ microparticle templates.[29−31] These involve loading of preformed capsules,[29] loading porous $CaCO_3$ microparticles prior to multilayer film assembly,[31] and

* To whom correspondence should be addressed. Phone: 318-257-5100. Fax: 318-257-5104. E-mail: mcshane@latech.edu.

† Max-Planck Institute of Colloids and Interfaces.

‡ Louisiana Tech University.

§ Current address: Interdisciplinary Research Centre in Biomedical Materials, Queen Mary University, E1 4NS, London, United Kingdom.

10.1021/bm050304j CCC: $33.50
Published on Web 02/18/2006

Scheme 1. Glucose Consumption in the Presence of GOx, Resulting in Gluconic Acid (GA) and Hydrogen Peroxide Production

$$\text{Glucose} + O_2 + H_2O \xrightarrow{GOx} GA + H_2O_2$$

Scheme 2. Hydrogen Peroxide Catalysis via Peroxidase, Yielding Oxygen and Water

$$H_2O_2 \xrightarrow{HRP} \frac{1}{2}O_2 + H_2O$$

"coprecipitation" involving preparation of $CaCO_3$ particles in the presence of the macromolecule to be encapsulated.[30] This latter approach results in the formation of a stable macromolecule−polyelectrolyte matrix inside the capsules following dissolution of the inorganic core.

Additionally, recent work has shown the utility of using other types of mesoporous materials such as mesoporous silica particles as supports for enzyme immobilization[13,32] and sacrificial templates to prepare enzyme-loaded polyelectrolyte microcapsules.[33] Both techniques have demonstrated high loading efficiency and retention of enzymatic activity; however, the methods involved in the preparation of mesoporous silica particles is a time-consuming process lasting several days,[13] and the process required for template dissolution requires the use of harsh chemicals, namely, hydrofluoric acid.[33]

A particularly attractive characteristic of the multilayer nanofilm microcapsules for biosensor applications is the capability to modulate capsule wall permeability, allowing macromolecular diffusion into and out of the capsule to be controlled.[27,34−36] The ability to control capsule permeability is critical to realization of enzyme-based sensors, which typically rely on reaction−diffusion kinetics of substrates and products. Controlling substrate diffusion from the bulk solution into capsules would allow precise kinetic regulation of the substrate-limited enzymatic reactions occurring within the microcapsule, resulting in desired sensor performance.[37] Local kinetic monitoring of reaction substrates and/or products, with respect to both space and time, would improve the understanding of the reaction and transport processes that occur within microcapsules, enabling improvement in system design.

A well-studied and documented sensing scheme for glucose involves exploiting the innate specificity of glucose oxidase (GOx) as the main sensing component (Scheme 1).[38] Several obstacles remain with traditional enzymatic glucose sensing schemes when attempting to construct microscale sensors, especially oxygen supply depletion and enzyme degradation caused by hydrogen peroxide and gluconic acid accumulation.[39] By incorporating horseradish peroxidase (HRP) into the sensing scheme, the hydrogen peroxide produced by glucose consumption is catalyzed into water and oxygen (Scheme 2), resulting in partial alleviation of these problems.[40] Therefore, it is hypothesized that a glucose sensor based on coupled catalysis of GOx and HRP could result in a greater range of sensitivity and longevity, since local concentrations of oxygen will be partially replenished and the rate of enzyme degradation will be decreased because of conversion of hydrogen peroxide before it attacks the GOx.

In this report, the encapsulation and characterization of a GOx and HRP coupled catalytic system within polyelectrolyte microcapsules is described as a step toward the production of microscale glucose sensing systems. Capsules containing entrapped enzymes were produced using polyelectrolyte capsules templated on enzyme-doped $CaCO_3$ microparticles.[30] The emphasis of this work is on the measurement of immobilized enzyme concentration within the microcapsules, the catalytic properties of the microcapsules, and the enzyme release properties of the capsules over time. The relationship between the respective GOx and HRP concentrations used during particle preparation and the enzyme concentration immobilized within the resulting capsules was also explored. Finally, real-time monitoring of glucose catalysis within the microcapsules was performed in an attempt to understand the spatial and temporal distribution of reactants and products. The results of this work are an essential step toward understanding the general behavior of enzymes in polyelectrolyte capsules, devices that have myriad biotechnological and medical applications, and a new method for analyzing these systems is presented. These findings also provide insight into the behavior of a glucose sensing scheme within the controlled volume polyelectrolyte microspheres, which will play a crucial role in the design and fabrication of fluorescence sensors.

Experimental Section

Materials. Poly(allylamine hydrochloride) (PAH, M_w 70 kDa) and poly(styrene sulfonate) (PSS, M_w 70 kDa) were obtained from Aldrich (Milwaukee, WI) for use in LbL film deposition. Glucose oxidase from *Aspergillus niger* (GOx, G6125), horseradish peroxidase (HRP, P8250), fluorescein isothiocyanate horseradish peroxidase (FITC HRP), and β-D-glucose were purchased from Sigma (St. Louis, MO). For fluorescence-based experiments, GOx was labeled with Oregon Green 488-X succinimidyl ester (OG, Molecular Probes, Eugene, OR), and Amplex Red reagent (Molecular Probes) was used for enzymatic activity experiments as well as real-time monitoring of glucose catalysis using confocal microscopy. A dialysis membrane with a molecular cutoff weight of 12.5 kDa (Sigma) was used to purify the enzyme conjugates. Calcium chloride dihydrate (Ultra, Sigma) and Na_2CO_3 (pro analysis, Merck, Germany) were used for $CaCO_3$ microparticle preparation. Following LbL film deposition, ethylenediaminetetraacetic acid (EDTA, Sigma) was used for core dissolution. Quick Start Bradford 1X reagent (1 L) was obtained from Bio-Rad Laboratories (Hercules, CA) and used to determine encapsulated protein concentrations. Ultrapure water with a resistivity greater than 18.5 MΩ, prepared by a three-stage Millipore Milli-Q Plus 185 purification system, was used for all experiments. Additionally, phosphate-buffered saline (PBS) tablets (Sigma) were dissolved in ultrapure water and used accordingly.

Synthesis and Characterization of Oregon Green 488-X-GOx (OG−GOx). For use in fluorescent imaging, OG−GOx was prepared using a 1:1 molar ratio of GOx and Oregon Green 488-X succinimidyl ester during the labeling reaction, which was performed using a standard amine labeling protocol.[41] Following OG−GOx synthesis, the activity of unlabeled GOx was compared to that of OG−GOx by continuously stirring 4.5 mL of 0.02 mg/mL of GOx and subsequently adding 0.5 mL of 100 mg/mL β-D-glucose. The pH of the solution was monitored as a function of time throughout the experiment, and the reaction was allowed to proceed for approximately 1.5 h, at which time a steady-state pH was observed. Following data collection, comparison between GOx and OG−GOx activity was performed using first derivative analysis of the linear region. All statistical analyses were performed using student's *t*-test with $\alpha = 0.1$.

Fabrication of Coprecipitated $CaCO_3$ Microparticles Containing GOx and HRP. Coprecipitated calcium carbonate microparticles containing GOx and HRP were fabricated through the rapid mixing of $CaCl_2$ and Na_2CO_3 solution in the presence of GOx and HRP (Figure 1). For this work, four distinct batches of coprecipitated particles were prepared using combinations of labeled and unlabeled enzyme species. This technique allowed the concentration of an individual enzyme species to be determined by using an unconjugated species and a separate fluorescently conjugated species in conjunction with fluorescence spectroscopy (e.g., OG−GOx and HRP to determine GOx concentration, or GOx and FITC−HRP to determine HRP concentra-

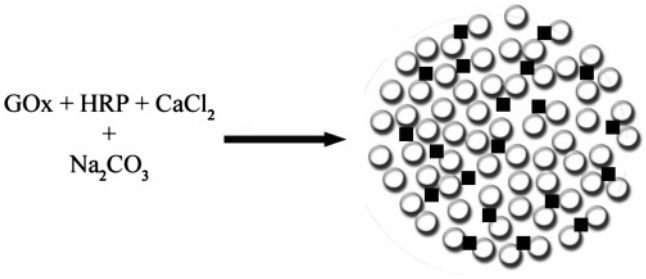

Figure 1. Fabrication process of coprecipitated microparticles. Black squares represent the adsorbed protein molecules within the porous volume of coprecipitated $CaCO_3$ microparticles, formed by aggregation of $CaCO_3$ nanoparticles.

tion). Different ratios of GOx and HRP were used during particle preparation to investigate the whether the initial GOx/HRP used during synthesis was correlated to the encapsulated GOx/HRP immobilized within the microcapsules.

The first batch of coprecipitated particles was produced using the following procedure: First, 7.5 mL of enzyme solution consisting of 5.0 mL of GOx solution and 2.5 mL of HRP solution (all protein concentrations were 10.0 mg/mL) was added to 7.5 mL of ultrapure water, which was continuously stirred at 650 rpm. Next, 5.0 mL of 1.0 M $CaCl_2$ was added to the solution, followed by the rapid addition of 5.0 mL of 1.0 M Na_2CO_3. After Na_2CO_3 addition, the reaction was allowed to proceed for 30 s under the stirred conditions (nucleation stage), after which the remainder of the crystallization procedure continued in static conditions (growth stage). This two-stage preparation technique is used to control the resulting size of the particles, where an increased nucleation time produces smaller-diameter particles and an increased growth time generates larger-diameter particles. Crystallization of $CaCO_3$ was performed at room temperature, and particle formation was monitored using a light microscope. Upon reaction completion, the newly prepared particles were centrifuged at 200 g for 3 min, followed by supernatant removal and subsequent resuspension in water. This washing procedure was repeated a total of three times to remove byproducts resulting from the precipitation reaction.

Two additional batches of coprecipitated particles were prepared using a similar procedure; however, the volume of conjugated and nonconjugated proteins varied as follows: (1) 5.0 mL of GOx solution, 2.0 mL of HRP solution, and 0.5 mL of FITC−HRP solution; (2) 2.5 mL of GOx solution, 2.5 mL of GO−GOx solution, and 2.5 mL of HRP solution. A batch of coprecipitated cores was also fabricated using a different initial GOx/HRP, such that 6.34 mL of GOx solution and 0.64 mL of HRP solution were used during synthesis. Additionally, a batch of particles was prepared in the absence of protein and used as a control for required experiments.

Polyelectrolyte Deposition. Prior to film adsorption, 2 mg/mL PAH and PSS solutions in 0.5 M NaCl were prepared, followed by pH adjustment to 6.5 using 1.0 M NaOH and 1.0 M HCl. Directly after the triple centrifugal washing, approximately 50 mg of coprecipitated $CaCO_3$ particles, which exhibit a net negative surface charge,[29−31] were suspended in PAH solution. Following a 15 min adsorption time, during which the particles were continuously shaken using a Vortex Genie-2 (Fisher Scientific International, Vernon Hills, IL) and protected from light with aluminum foil, the particles were rinsed using quadruple centrifugal washing with 0.05 M NaCl and subsequently resuspended in PSS solution. Following addition of PSS, one bilayer of PAH and PSS ({PAH/PSS}) was deposited onto the coprecipitated particles. This sequential process was continued, until a film comprising eight bilayers of PAH/PSS (denoted as $\{PSS/PAH\}_8$) was assembled onto the templates. The final washing step was carried out using ultrapure water.

Microcapsule Preparation. Following multilayer film deposition, the microparticles were suspended in 0.1 M EDTA (pH 7.0, using 1 M HCl/NaOH) to dissolve the carbonate templates. While suspended in 0.1 M EDTA, the solution was continuously shaken for 30 min while also minimizing light exposure. The suspension was then centrifuged at 1500 g for 5 min, followed by supernatant removal and subsequent resuspension in 0.1 M EDTA solution. This process was repeated until a total of three treatments with EDTA were achieved. The capsule solution was then washed four times with ultrapure water, using the same centrifugation protocol. The resulting capsule suspension was stored at 4 °C in water until needed.

Scanning electron microscopy (SEM) imaging was performed for particles prepared in the absence of protein, for coprecipitated particles, and for the resulting capsules. Sample preparation involved placing a 5 μL drop of capsule suspension on a glass slide followed by drying with nitrogen gas. Gold sputtering of the samples was performed, and images were obtained using a Leo Gemini 1550 with an operating voltage of 3 keV.

Following capsule preparation, confocal laser scanning microscopy (CLSM) imaging was performed using a Leica TCS I imaging system with a 100× oil immersion objective (NA = 1.4). The microcapsules containing OG−GOx and FITC−HRP were excited using 488 nm ArKr excitation. Emission data was collected over a 500−600 nm band.

Calculation of Amount of Protein Encapsulated within Polyelectrolyte Microcapsules. Experiments were performed to determine the amount of GOx and HRP encapsulated per microcapsule as well as investigate how the protein ratios used during particle preparation are related to the encapsulated protein ratio. Prior to determining the respective encapsulated protein concentrations, the concentration of capsules within the stock suspension was determined using a bright-line hematocytometer (cell-counting chamber, Sigma). Ten individual measurements were performed on each suspension, followed by the calculation of the average capsule concentration and standard deviation. Additionally, the size distributions of particles within each batch were determined using transmission and fluorescence confocal line scan analysis of 50 objects within each population, followed by mean and standard deviation calculation.

The concentrations of GOx and HRP entrapped within the microcapsule were determined using both fluorescence analysis and the Bradford protein assay. The fluorescence method was performed to determine the individual concentration of GOx and HRP, while the Bradford assay was performed to determine the collective protein concentration. Theoretically, the sum of the GOx and HRP concentrations as determined by the fluorescence method should match the Bradford results.

For the fluorescence technique, capsules fabricated containing unlabeled HRP and OG−GOx were analyzed by removing 100 μL of stock suspension and adding 100 μL of 0.1 M NaOH, resulting in capsule dissociation and ultimately a homogenized polymer-protein solution.[42,43] This solution was then added to 2.8 mL of 0.25 M PBS, pH 7.4. Standard solutions containing a known amount of OG−GOx were prepared, ranging in concentration from 0.2 mg/mL to 1.3 μg/mL. It is important to note that the fluorescence spectra of both OG−GOx and FITC−HRP are sensitive to changes in pH; therefore, standards were carefully prepared to ensure that pH values remained constant. A background signal was collected using dissolved $\{PSS/PAH\}_8$ capsules fabricated on $CaCO_3$ microparticles, which were prepared without the addition of protein solution, allowing the contribution of microcapsule components as a baseline measurement to be established. Following sample preparation, spectral acquisition was performed using the Spex Fluorolog II dual monochromator based spectrometer, with 495 nm excitation light and 500−550 nm emission collection band. A calibration curve was prepared to relate emission intensity at 520 nm to OG−GOx concentration. The emission intensity obtained from the dissolved capsule suspension was compared to the calibration curve, allowing the protein concentration within the dissolved capsule solution to be determined. These data were normalized to the number of capsules present in the sample, resulting in approximation of the GOx concentration per capsule. A similar procedure was performed to determine the amount of HRP encapsulated within the microcapsules. However, 488 nm excitation light was used during emission spectrum acquisition of FITC−HRP. Additionally, to confirm

the results obtained from the fluorescence method, the protein concentration was furthermore determined using the Bradford protein assay.

The total encapsulated protein concentration was determined using the Bradford protein assay, which involved using microcapsules containing unlabeled GOx and HRP for analysis. Specifically, 2 μL of capsule suspension was removed and added to 100 μL of 0.1 M NaOH. This solution was then added to 800 μL of Quick Start 1X Bradford reagent. Standards were prepared using a protein solution comprising 2 GOx/1 HRP, with a final concentration of 1 mg/mL. Controls were also prepared using the following: (1) 1 mg/mL of 2 GOx/1 HRP and 0.5 mg/mL of PSS and PAH and (2) 0.5 mg/mL PSS and PAH, allowing for the correction of polyelectrolyte contributions to the resulting spectra. Following reagent addition, the samples were stirred for 5 min. Absorbance spectral acquisition was performed using a Cary 400 (Varian GmbH, Germany) UV−visible spectrophotometer over 450−700 nm. A calibration curve was prepared using the absorbance measurement obtained at 595 nm, and the protein concentration of the capsule suspension was determined after accounting for polyelectrolyte contribution. The total protein concentration per capsule was obtained by normalizing the results to the number of capsules present within the sample.

Determination of Protein Release Properties. The time-dependent release properties of GOx and HRP were determined in order to quantify the stability of protein immobilization within the microcapsule structures and apparent differences in release properties between the enzyme species. The respective release properties of GOx and HRP from the microcapsules were determined using fluorescence analysis. To acquire the release data for GOx, capsules containing unlabeled HRP and OG−GOx were used. In particular, 500 μL of stock capsule solution was diluted with 1 mL of ultrapure water and the pH adjusted to 7.0 using 1 M NaOH and/or HCl. The sample was centrifuged at 1500 g for 10 min, followed by removal of 1 mL of supernatant. The fluorescence spectrum of the supernatant was collected using 495 nm excitation and 500−550 nm emission. Three subsequent measurements were performed during data acquisition for each time point, followed by supernatant replacement. This procedure was repeated daily for approximately 20 days. Standards containing a known amount of OG−GOx were prepared, ranging in concentrations from 1.3 μg/mL to 0.2 mg/mL, resulting in an emission intensity−protein concentration calibration curve. Comparison of the supernatant emission data to the calibration curve allowed the concentration of GOx released into the supernatant to be determined. Upon normalizing to the number of capsules present in each sample, the amount of protein released per capsule was estimated and compared to the original concentration obtained as previously discussed. A release profile was constructed by plotting the emission maxima versus time. A similar procedure was performed using microcapsules containing unlabeled GOx and FITC−HRP to determine the release profile of HRP; however, 488 nm excitation was used. The profiles were fitted in MATLAB using standard $1 - e^{-kt}$ release kinetics.

Catalytic Properties of Encapsulated versus Free Enzyme. A comparison of encapsulated and free enzyme catalytic properties was performed using microcapsules containing unlabeled GOx and HRP and solution containing unlabeled GOx and HRP, respectively. This comparison was performed to quantify how enzyme immobilization within the controlled volume of the microspheres influences the kinetics of glucose catalysis. To monitor the enzymatic activity of the GOx and HRP coupled catalytic system, Amplex Red, a nonfluorescent HRP substrate that is converted to a fluorescent product, resorufin, and atmospheric oxygen in the presence of hydrogen peroxide and HRP, was employed. When glucose consumption is the limiting step in the reaction scheme, each mole of glucose consumed results in the production of 1 mol of resorufin. A solution containing 100 μM Amplex Red was prepared in 0.25 M PBS (pH 7.4, using HCl/NaOH) to stabilize the pH of the system. Prior to enzymatic activity analysis of the encapsulated enzyme species, the capsules were washed with ultrapure water (1500 g for 10 min) to remove released enzyme present in the supernatant. A 10 μL volume of stock capsule suspension, containing encapsulated unlabeled species of GOx and HRP, was added to 2.8 mL of 100 μM Amplex Red solution. The suspension was placed in the fluorimeter and continuously stirred during measurement of resorufin emission ($\lambda_{ex} = 560$ nm and $\lambda_{em} = 590$ nm), and spectra were gathered with respect to time. Following the establishment of initial steady-state intensity, 100 μL of 100 μM β-D-glucose was added to the stirred suspension, and the reaction was allowed to proceed for approximately 1 h. After data collection, activity values were collected from slope analysis of the linear activity range. A similar procedure was performed using enzyme in free solution. The protein solution used during analysis of free enzyme activity comprised a 2 GOx/1 HRP mass ratio, with total concentration of 1 mg/mL. The ratio of enzymes used to prepare the free enzyme solution and mass of free enzyme added during activity analysis was approximately equal to that contained within the microcapsule suspension, as determined by fluorescence and the Bradford assay analysis.

Effect of Polyelectrolytes on Enzymatic Activity. The enzymatic activity of protein in free solution was acquired following a similar procedure as detailed above. This comparison was performed in order to determine if in the presence of the PSS and PAH, GOx and HRP activity is influenced by interference with the active site, thus affecting the kinetics of glucose catalysis. A sample containing protein (2 GOx/1 HRP, with a final concentration of 1 mg/mL) and polyelectrolyte (0.5 mg/mL PAH and PSS) was prepared. Using this solution, a fluorescence-based activity test was performed as described above. A control was prepared using only protein solution containing 2 GOx/1 HRP, with a final concentration of 1 mg/mL. The effect of polyelectrolyte on the enzymatic activity was performed by evaluating the slope of the linear activity region of both profiles. It should be noted that PAH was added to the protein solution, followed by the addition of PSS to prevent immediate polyelectrolyte complexation, as would have occurred if a mixture of PAH and PSS was prepared prior to the addition of the protein solution.

Real-Time Monitoring of Glucose Catalysis within Polyelectrolyte Microcapsules. Real-time imaging of glucose catalysis was performed to understand the spatial and temporal distribution of glucose consumption within the microcapsule constructs. For real-time glucose catalysis monitoring, a 25 μL of microcapsule stock suspension containing unlabeled GOx and HRP was added to 100 μL of 100 μM Amplex Red solution prepared in 0.25 M PBS (pH 7.4, adjusted using HCl/NaOH) and incubated overnight. Prior to analysis, the capsule suspension was washed (1500 g for 10 min) to remove released enzyme and resuspended with the same Amplex Red solution. CLSM analysis was used to spatially monitor glucose catalysis by observing the formation of resorufin with respect to time, following glucose addition. The temporal production of fluorescent resorufin was monitored using 542 nm HeNe laser excitation and 560−620 nm and emission collection. This procedure was performed by placing 10 μL of capsule/Amplex Red suspension on a no. $1^1/_2$ 24 × 60 mm^2 cover glass (VWR Scientific, West Chester, PA), followed by the addition of 1 μL of 85 μM β-D-glucose during image acquisition. Images were collected every 15 s using five line scan averages per acquired image for a total measurement time of 1185 s.

Examination of spatial glucose consumption was performed using region of interest (ROI) analysis. This method involved defining a common spatial ROI of circular geometry in the acquired images and analyzing the fluorescence emission intensity normalized to the total number of pixels within the ROI with respect to time. These data result in a graphical representation of the average temporal fluorescence intensity within the ROI. Three ROIs were used for analyzing the change in resorufin fluorescence with respect to time: an ROI containing the entire capsule (including the capsule walls), an ROI within the capsule interior (not including the capsule walls), and an ROI within the supernatant (used as a control). The positions of these ROIs are shown in Figure 2.

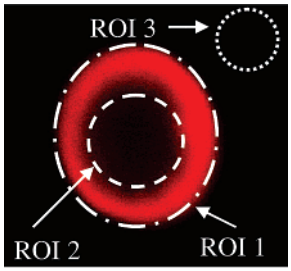

Figure 2. CLSM image of resorufin fluorescence resulting from glucose oxidation and the ROIs used to analyze resorufin production with respect to time. ROI 1 contains the entire capsule, ROI 2 contains only the capsule interior, and ROI 3 contains an external region representative of the local environment.

Results and Discussion

Effect of Labeling on GOx Activity. Following OG−GOx synthesis, the activity of OG−GOx was compared to that of unlabeled GOx to determine if the catalytic properties of GOx were altered as a result of dye conjugation. On the basis of first-order derivative analysis of the linear activity range, the results indicate less than 10% difference between the catalytic activity of the native (-1.2×10^{-3} pH units/s) and unlabeled (-1.1×10^{-3} pH units/s) enzyme species. As expected, the enzymatic activity of the labeled enzyme is not significantly affected by dye conjugation because of the seven-atom spacer between the succinimidyl ester and the fluorophore, which minimizes fluorophore interaction with the enzyme active site.

Microcapsule Characterization. By preparing carbonate cores in the presence of GOx and HRP, it is possible to capture the protein within the $CaCO_3$ particles. The enzyme molecules are immobilized through surface adsorption onto the $CaCO_3$ nanoparticles formed during the nucleation phase, and following subsequent aggregation in the growth phase, the enzymes remain adsorbed on the interior matrix of the porous $CaCO_3$ microparticles (Figure 1).[31] Following template synthesis, sequential adsorption of the desired PAH/PSS bilayers results in a network of polyelectrolyte branches within the porous template. Upon template dissolution, the protein molecules adsorbed to the internal architecture of the $CaCO_3$ microparticles are released and electrostatically bind with both the interpenetrating polyelectrolyte matrix and the polyelectrolytes of the capsule walls. This process is illustrated in Figure 3.

SEM images of the coprecipitated templates show that the porous nature of the cores is maintained when enzyme molecules are introduced during template preparation (Figure 4A). Prior to drying and image collection, a template sample was pulverized using a glass slide such that some of the templates were broken, allowing internal structure analysis. As shown in Figure 4B, the porous characteristic of the coprecipitated particles is caused by nanoparticle aggregation; however, when compared to the structure of $CaCO_3$ cores synthesized in absence of enzyme molecules, the coprecipitated cores exhibit a decreased pore diameter.[29,30] As previously reported, calcium carbonate crystal growth is retarded in the presence of protein.[44] Therefore, it is reasonable to conclude that the diameter of $CaCO_3$ nanoparticles formed during the nucleation phase of crystallization in the presence of GOx and HRP will be smaller in diameter than nanoparticles prepared in the absence of protein. During the nanoparticle aggregation process, which ultimately forms the $CaCO_3$ microparticles, the smaller-diameter nanoparticles will form microparticles comprising more densely packed nanoparticles, resulting in decreased porosity when compared to the porosity of $CaCO_3$ particles prepared in the absence of protein. This observation was quantified in previous reports, which indicate that $CaCO_3$ prepared in the presence of protein molecules, exhibited pore diameters in the range 10−40 nm, whereas the pore diameter of particles prepared in the absence of protein was determined to be 20−70 nm.[29,30]

Following the deposition of $\{PAH/PSS\}_8$ onto the templates, SEM imaging was performed. As a result of polyelectrolyte deposition, the surface roughness of the coated microcapsule (Figure 5A) is reduced in comparison of that of the initial microparticles (Figure 4A,B), which was also observed in previous studies.[29,30] EDTA has been shown to remove 99.98% (w/w) of the carbonate template[24] by forming a water-soluble complex with Ca^{2+} ions, resulting in microcapsule formation (Figure 5B). The rough nature of the capsule caused by the rough surface morphology of the core templates and thick defined folds composing the capsule walls resulting from $\{PAH/PSS\}_8$ deposition are also evident in Figure 5B. The surface morphology of the particles and capsules obtained in this study are in good agreement with previous work performed using a similar method.[29]

Following dissolution, the protein distribution within the microcapsule was analyzed using CLSM. The resulting CLSM

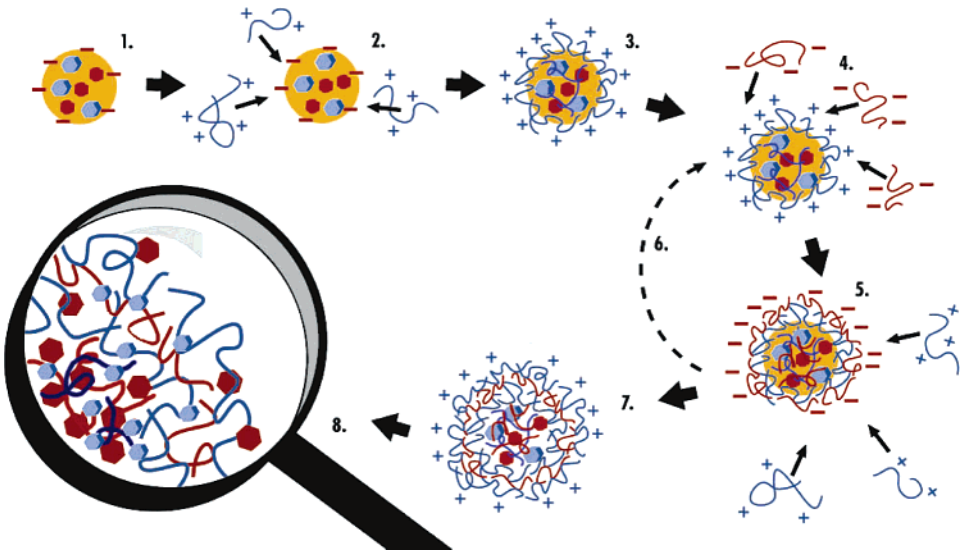

Figure 3. Schematic depiction GOx (red hexagons) and HRP (blue hexagons) immobilized within coprecipitated templates (yellow). Infiltration of PAH (red) and PSS (blue) form a matrix to which GOx and HRP are immobilized following core dissolution with EDTA.

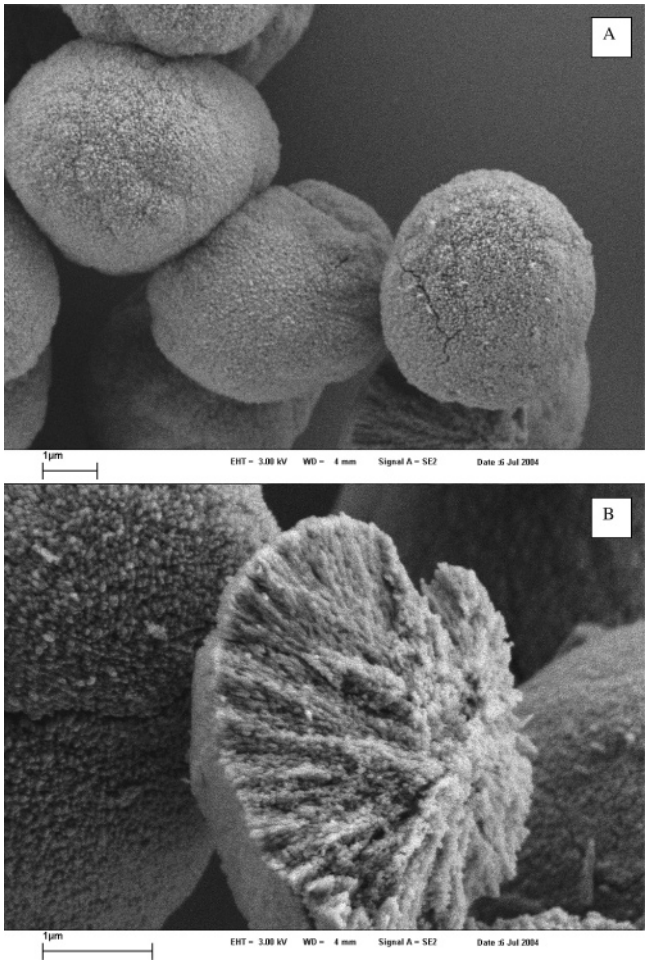

Figure 4. SEM images of $CaCO_3$ microparticles prepared in the presence of GOx and HRP (A) and internal structure of coprecipitated microparticles (B).

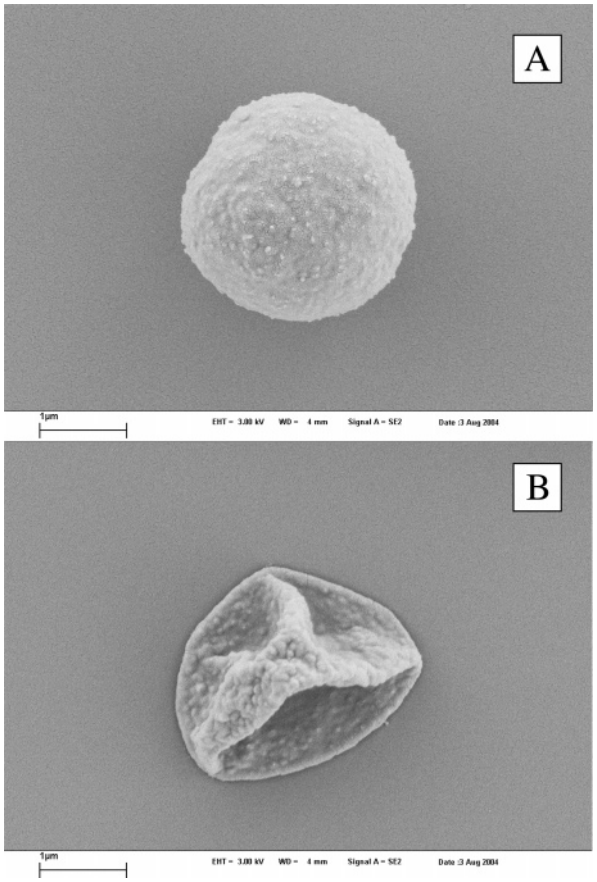

Figure 5. SEM images of coprecipitated microparticles after {PAH/PSS}$_8$ deposition (A) and resulting polyelectrolyte microcapsule following template dissolution (B).

images and the corresponding line scan data are presented in Figure 6. The protein distribution in both cases tends to be heavily localized within the capsule walls, although both enzymes are also present within the center of the capsule. Additionally, line scan analysis shows that an approximate fourfold increase in GOx and HRP concentration is observed within the capsule walls when compared to that of the capsule interior. Nonhomogeneous protein distribution within the microcapsules can be attributed to the random formation of the interpenetrating polyelectrolyte matrix with which the enzymes form complexes.[29] The accumulation of macromolecules within the polyelectrolyte network has been previously observed[29−31] and has been attributed to the electrostatic interactions between the free charge sites of the polyelectrolytes and the macromolecules. Under neutral conditions, GOx is negatively charged (pI $\approx$ 5.5)[45] and would therefore interact with the nonneutralized amine residues of PAH. However, HRP is positively charged (pI $\approx$ 8.8) under neutral conditions and would interact with the uncompensated sulfonate residues of PSS.[14] Additionally, given opposite net charge, there is the possibility of GOx−HRP complexation within the capsule architecture, which could occur during particle preparation or following template dissolution.

To determine the amount of protein immobilized within the microcapsules, two techniques were used: fluorescence spectroscopy and standard Bradford protein assay analysis. Using the fluorescence technique, the emission spectra of standards containing known concentrations of OG−GOx and FITC−HRP were acquired as previously discussed in the Experimental Section. Following microcapsule dissolution at high pH, the emission spectra of dissociated capsules containing unknown concentrations OG−GOx and FITC−HRP were collected and compared to the spectra of the respective standards. Hemocytometer results indicate that the capsule concentration within the various capsule suspensions was approximately 10^9 capsules/mL. Particle sizing analysis obtained from capsules containing OG−GOx and FITC−HRP yield average diameters of 6.4 $\pm$ 0.33 μm and 3.0 $\pm$ 0.22 μm, respectively, and 2.7 $\pm$ 0.25 μm for capsules containing unlabeled GOx and HRP. It should be noted that, although a similar fabrication method was used during particle preparation, batch-to-batch variation still remains a problem and was observed in a previous study.[29] Although significant batch-to-batch diameter variation was apparent, less that 10% variation within each batch was observed and was accounted for using error propagation statistics. By normalizing the data to the number of capsules present within the sample and the capsule volume, the average concentration of each respective enzyme within the microcapsules was calculated. When using microparticles prepared with a 2 GOx/1 HRP mass ratio (0.55 GOx/1 HRP mole ratio), the average mass of immobilized enzyme was determined to be 4.27 $\pm$ 0.05 pg/capsule, and the corresponding concentrations of encapsulated enzyme were determined to be 29.4 $\pm$ 3.6 mg/mL (668.1 $\pm$ 81.8 μM) for HRP and 13.7 $\pm$ 1.0 mg/mL (85.6 $\pm$ 0.63 μM) for GOx. Thus, the encapsulated ratios of GOx/HRP were 0.46:1 mass concentration and 0.128:1 mole concentration, respectively. However, when using particles prepared with a 10 GOx/1 HRP mass ratio (2.75 GOx/1 HRP mole ratio), the resulting encapsulated ratios of GOx/HRP were 3.02:1 mass concentration and 0.83:1 mole concentration, respectively. To confirm these

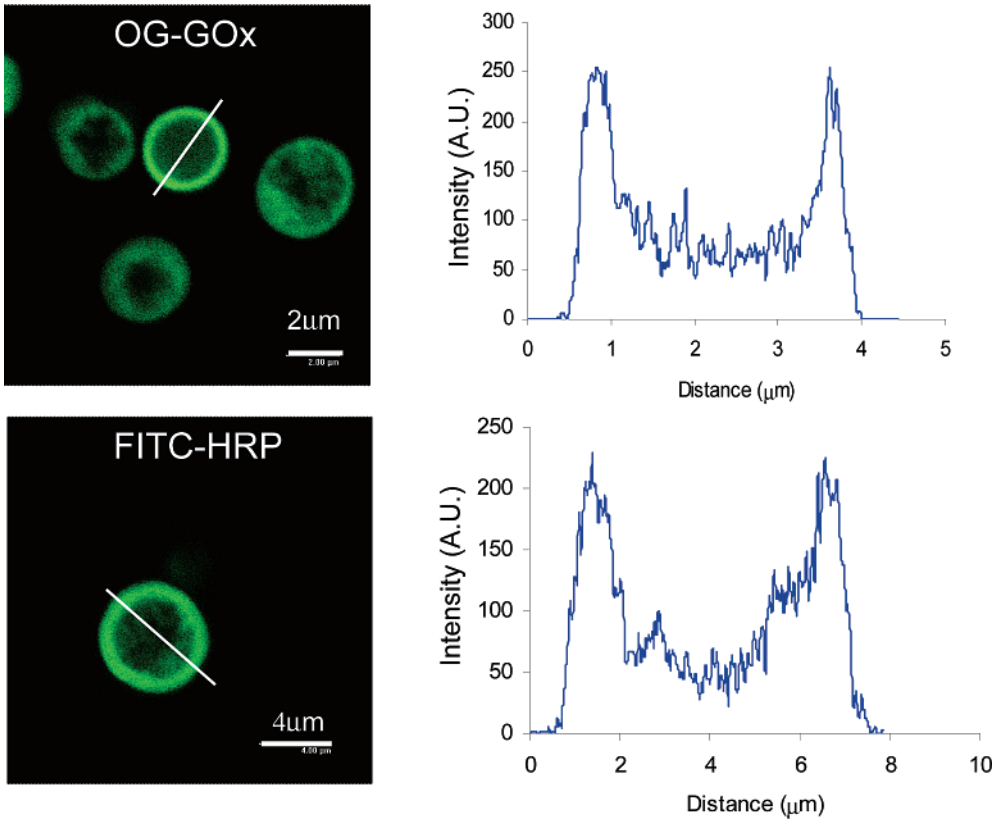

Figure 6. Typical CLSM images of microcapsules containing unlabeled HRP and OG−GOx and microcapsules containing FITC−HRP and unlabeled GOx, with the corresponding line scan data to the right.

results, a Bradford assay was performed on the microcapsules prepared using 1 GOx/2 HRP mass ratio. The measurements indicated that 4.21 ± 0.5 pg of enzyme per capsule was encapsulated, in agreement with values obtained using the fluorescence method.

These results confirm several important findings. First, the GOx/HRP ratio used during template synthesis is not equal to the GOx/HRP encapsulated within the microcapsules; particularly, HRP is more efficiently adsorbed during particle preparation than GOx. A reasonable explanation for the greater adsorption affinity of HRP during particle preparation when compared to GOx is the electrostatic binding of the oppositely charged $CaCO_3$ and HRP molecules during particle synthesis. Additionally, these results indicate that, by changing the GOx/HRP during particle synthesis, the GOx/HRP within the microcapsules can be changed, indicating that some degree of control might be attainable; however, further studies are necessary to establish a clear relationship between initial protein ratio and encapsulated protein ratio.

To examine the effect of encapsulation on enzymatic activity, the catalytic profile of microcapsules containing unlabeled GOx and HRP was compared to that of GOx and HRP in solution (Figure 7A). Since an approximate 1 GOx/2 HRP mass ratio was determined to exist within the microcapsules, a solution containing a similar ratio and concentration was prepared for the activity analysis of the free enzyme solution. The concentration of protein used in the control was determined by calculating the concentration of capsules within the activity sample, then taking the product of the number of capsules and the protein concentration per capsule.

For activity analysis, the raw activity data were modeled using standard linear regression so that the enzymatic activity could be quantified. Linear regression analysis indicates that the enzyme-coupled system within the microcapsules exhibits 15% ± 2% of the activity of the free counterpart, a decrease in effective activity of approximately 85%. It is common for immobilized enzymes to lose some degree of activity; this is usually attributed to physical blocking of the substrate binding site when immobilized within polyelectrolyte capsules/multilayers.[15,22,31] In this case, a substantial loss of apparent activity may also be attributed to diffusion limitations of glucose within polyelectrolyte multilayers comprising PSS and PAH: The diffusion coefficient of glucose through films comprising $\{PSS/PAH\}_7$ multilayers on porous substrates has been reported to be 9.87×10^{-10} cm^2 s^{-1}, a decrease of 4 orders of magnitude when compared to glucose diffusivity in water (6.9×10^{-6} cm^2 s^{-1}).[46] Overall, the polyelectrolyte membrane functions as a substrate diffusion barrier, which greatly hinders the transport of glucose to the immobilized enzymes within the capsule, resulting in a net loss of effective enzymatic activity.

The effect of the polyelectrolyte presence on enzymatic activity was studied in order to further understand why a loss of 85% enzymatic activity was observed for encapsulated GOx and HRP when compared to GOx and HRP in solution. Following data acquisition, the raw data were analyzed using standard linear regression, and the slopes of the linear activity region were compared (Figure 7B). The control used for comparison represented the enzymatic activity of GOx and HRP, whereas the sample consisted of GOx and HRP in the presence of PAH and PSS, both of which were performed in solution. It should be noted that the mole concentration of polyelectrolyte used was in excess of the mole concentration of protein in solution for all cases. Following analysis using standard linear regression, the slopes of the linear activity region were compared. The activity of the control was determined to be 0.0595 AU/s and the activity of GOx and HRP in the presence of PSS and PAH was determined to be 0.0600 AU/s. These data indicate that there is less than a 1% difference between

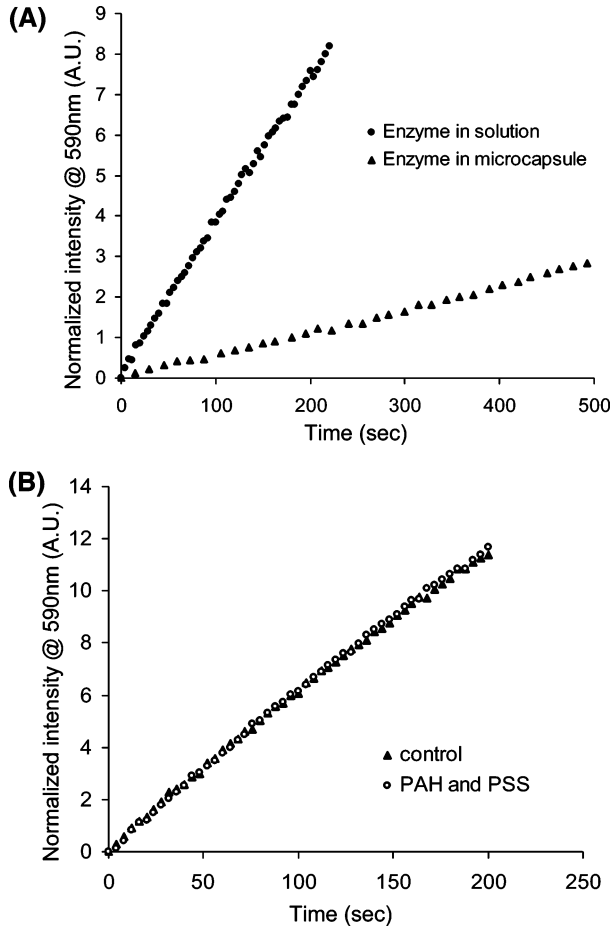

Figure 7. (A) Comparison of enzymatic activity of enzymes in solution (●) and enzymes immobilized within polyelectrolyte capsules (▲). (B) Enzymatic activity of GOx and HRP (▲) and GOx and HRP in the presence of PSS and PAH (○) in solution.

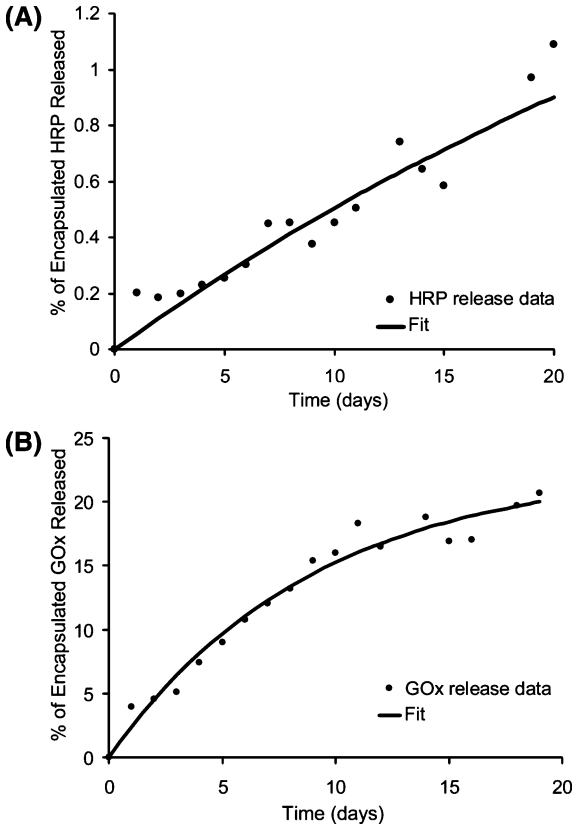

Figure 8. (A) Release profile of GOx from $\{PAH/PSS\}_8$ microcapsules templated on coprecipitated $CaCO_3$ microparticles. (B) Release profile of HRP from $\{PAH/PSS\}_8$ microcapsules templated on coprecipitated $CaCO_3$ microparticles.

the catalytic properties of the coupled catalytic system when in the presence of PAH and PSS, indicating that the polyelectrolyte effect on enzymatic activity is negligible.

Additionally, reports indicate that polyelectrolyte films minimally affect hydrogen peroxide transport,[47] making it reasonable to conclude that hydrogen peroxide should be able to freely diffuse within the capsules and would therefore not be a limiting step in the reaction process. Even though the mole ratio of GOx/HRP within the capsules is 1.28:1, indicating that there is a surplus of GOx molecules, the molar turnover numbers for the enzyme species used in this study are 3.2×10^9 and 9.7×10^9 units/mol for GOx and HRP, respectively; therefore, HRP is approximately 3 times more catalytically active than GOx and therefore is not expected to be a limiting step in glucose catalysis. This further implies that the limiting step within the encapsulated GOx and HRP coupled catalytic system is glucose diffusion, and that diffusion limitations through the polyelectrolyte complex substantially contribute to the apparent loss of capsule enzymatic activity.

The time-dependent release of GOx and HRP from polyelectrolyte microcapsules was quantified using fluorescence spectroscopy. The emission spectra acquisition of the respective capsule supernatants (capsules containing OG−GOx and unlabeled HRP and capsules containing unlabeled GOx and FITC−HRP, respectively) following centrifugation was performed. The release profiles obtained are given in Figure 8. The data presented were normalized at each time point to an intensity standard to account for temporal fluctuations in the instrumentation. These data were modeled using the following release equation, which has previously been used to describe macromolecular diffusion in polyelectrolyte microcapsules

$$\text{release}(t) = 1 - e^{-kt}$$

where k represents the fitting parameter. [48]

With the equation described above, a fit with R^2 of 0.985 was obtained for the GOx release profile. These data determine that approximately 35 pg of GOx per capsule was released from the capsule over a period of 19 days, indicating a loss of approximately 20% ± 3% GOx into the supernatant over that time period. However, following similar analysis of the microcapsules containing unlabeled GOx and FITC−HRP, the results show that only 2 pg of HRP per capsule was released into the supernatant over the same time period, indicating a loss of 0.9% ± 0.2% HRP, only about 6% of the amount of GOx released from the capsule. However, it is important to note that release data were obtained through analysis of the fitting equations, and although the R^2 value of the fitting equation used to describe HRP release was 0.952, low emission signals were present during the acquisition of HRP leaching data. The low signal levels were due to the small amount of HRP released into the supernatant, and the noise in the data translated into larger uncertainties in the fitting parameter.

Interestingly, the release data also suggest that GOx (M_w = 160 kDa), although larger than HRP (M_w = 44 kDa), is released from the microcapsules at a higher rate. A possible explanation for this finding involves electrostatic binding kinetics of the proteins during template dissolution and release monitoring. However, protein−polyelectrolyte interactions are complex and arise from van der Waals forces, dipolar or hydrogen bonds,

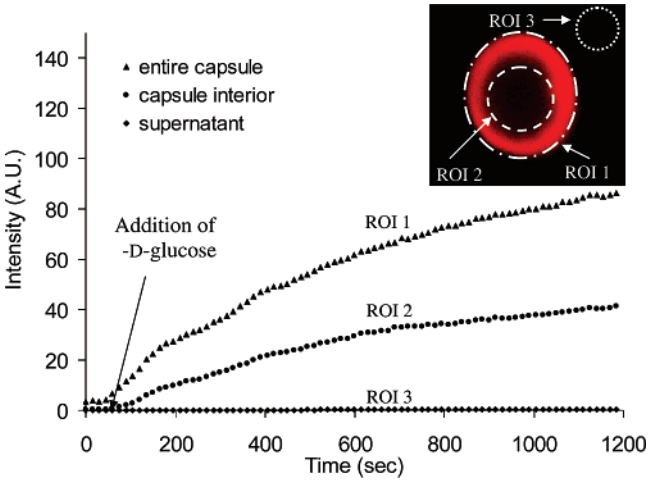

Figure 9. Real-time catalytic monitoring of glucose within the entire capsule (▲, ROI 1), the capsule interior (●, ROI 2), and the supernatant (◆, ROI 3).

electrostatic forces, and hydrophobic effects[49] and involve a range of parameters including the pH and ionic strength of the solution.[50] Of these, electrostatic interactions are considered to play the major role. Since the pH during template dissolution and release monitoring was controlled (pH = 7.0) and the pI values of GOx and HRP are 5.5 and 8.8, respectively, both enzymes will exhibit a net charge.[49,51] However, HRP will exhibit a twofold greater charge density than GOx, due to a greater difference between the pI of HRP and the pH of the environment. As previously reported, when like molecules with varying charge densities are adsorbed to separate surfaces, those with a low charge density are more easily desorbed from the surface when compared to like molecules with a greater charge density.[52,53] With a higher charge density than GOx, HRP will have a greater number of charged sites available to electrostatically bind to the surrounding nonneutralized polyelectrolyte sites in the capsule wall and the interior matrix. Therefore, it is likely that HRP forms a stronger electrostatic bond with the surrounding polyelectrolyte complex, resulting in a decreased release rate when compared to that of GOx. Additionally, the molar concentration of HRP within the microcapsules, 668.1 ± 81.8 μM, was greater that that of GOx (85.6 ± 0.63 μM), suggesting that greater concentration gradients exist to drive unbound HRP molecules from the capsule interior. Even though greater diffusion forces are exerted on HRP, only 6% of HRP is released when compared to GOx, supporting stronger protein−polyelectrolyte binding with HRP.

As mentioned, glucose is readily catalyzed into H_2O_2 in the presence of GOx and O_2, and nonfluorescent Amplex Red is subsequently catalyzed into fluorescent resorufin and oxygen in the presence of HRP and H_2O_2. Given the previous data, which point to glucose diffusion and consumption as the rate-limiting step, it can be assumed that for every mole of glucose consumed, 1 mol of resorufin is produced for a given point in time. Therefore, the spatial and temporal production of resorufin can be viewed as a direct representation of glucose consumption. Monitoring of spatial and temporal consumption of glucose within the microcapsules was performed using time-based CSLM image acquisition of resorufin production following β-D-glucose addition at 35 s (Figure 9). Following time-based image acquisition, the intensity changes within several ROIs were analyzed to give insight on spatial glucose catalytic characteristics. The temporal intensity profile of each ROI and a typical CLSM image of a microcapsule following the addition of β-D-glucose are depicted in Figure 9, where an increase in red fluorescence results from resorufin production.

Upon comparison of the temporal intensity of ROI 1 to ROI 2, it is apparent that the majority of glucose catalysis occurs within the walls of the microcapsule, as indicated by the greater rate of temporal resorufin production along with the greater concentration of resorufin produced within the capsule walls. Increased glucose catalysis within the capsule wall was expected because of the greater concentration of enzyme immobilized within the capsule walls when compared to the concentration of enzyme immobilized within the interior matrix (Figure 6). However, glucose consumption also occurs within the microcapsule as indicated by the temporal catalytic profile obtained from ROI 2. Glucose catalysis occurring within ROI 2 further indicates that the consumption of glucose is the limiting reaction step, because as glucose is introduced, GOx immobilized within the capsule walls reaches maximum velocity, allowing additional glucose molecules to diffuse past and enter the capsule interior before being consumed. Additionally, negligible glucose consumption occurs within the supernatant (ROI 3), indicating the absence of released enzyme.

From a similar analysis, when comparing ROI 1 and ROI 2, it appears that approximately twice the quantity of glucose is catalyzed in the capsule walls when compared to the catalysis occurring within the microcapsule. This observation was determined by comparing the fluorescent intensities of ROI 1 (86.2 AU) to ROI 2 (41.5 AU) collected at 1200 s. The initial activity, as indicated from the slope of the catalytic profile from 30 to 200 s, for the entire capsule (0.165 AU/s) is approximately 2.4 times greater that that of the capsule interior (0.070 AU/s). By subtracting the interior activity from the total capsule activity, an activity of 0.095 AU/s is determined, suggesting that the rate of glucose consumption within the capsule walls is approximately 1.35 times greater than that of the capsule interior. Greater enzymatic activity within the walls of the microcapsule can be attributed to the high concentration of GOx and HRP present within the capsule walls as indicated by initial CLSM imaging of enzyme distribution (Figure 6), which in turn limits the amount of glucose able to diffuse into the capsule interior.

Line scans of the CLSM images obtained for enzyme distribution analysis show the ratio of average capsule wall intensity to average capsule interior intensity to be 4.09, indicating that the concentration of enzyme within the capsule walls is approximately four times that of the capsule interior. However, similar analysis of the image acquired at 1185 s (Figure 9) during spatial and temporal glucose consumption analysis yields a ratio of 6.67. Assuming that the immobilized enzymes within the capsule wall and interior are able to consume glucose and produce resorufin at a similar rate, differences in fluorescence attributed enzyme presence (Figure 6) and glucose consumption and resorufin production (Figure 9) are indicators of the spatial and temporal concentrations of catalytically active enzyme. The higher ratio associated with images used to analyze resorufin production indicate that a significant population of the enzyme localized within the capsule interior is catalytically inactive or inaccessible. These data complement the previous findings, again suggesting that substrate diffusion limitations exist within the current system, because the polyelectrolyte nanofilms and peripheral consumption due to high enzyme concentration within the capsule walls limits the total reaction that occurs within the capsule interior.

Conclusion

The characterization of a coupled catalytic system consisting of GOx and HRP within cosynthesized $CaCO_3$ cores has been reported. Results indicate that, by synthesizing $CaCO_3$ cores in the presence of GOx and HRP, $CaCO_3$ microparticles containing GOx and HRP can be obtained. These microparticles can then be used as sacrificial templates for the preparation of polyelectrolyte microcapsules. Upon template dissolution, the adsorbed GOx and HRP are released and subsequently bind to the interpenetrating polyelectrolyte matrix by electrostatic interactions, thus resulting in microcapsules containing GOx and HRP. The encapsulated enzymes are active and readily catalyze glucose within the capsule interior and within the capsule walls; however, enzymatic activity of the encapsulated coupled enzyme systems is significantly lower that that of the enzyme system activity in solution. Results indicate that polyelectrolyte complex interaction with enzyme molecules have a negligible effect on enzymatic activity, further emphasizing substrate diffusion limitations caused by a high enzyme concentration within the capsule walls and substrate diffusion limitation through the capsule walls. However, for enzymatic-based sensing systems, it is essential that the sensing scheme be analyte-limited, allowing the system to effectively transduce signals solely on the basis of analyte variation, illustrating the ability of LbL coating to alter analyte diffusion properties. Additionally, real-time monitoring of glucose consumption within the microcapsules was performed, which indicated that the majority of glucose catalysis occurred within the capsule walls when compared to that of the capsule interior. Although the current system shows promise for potential application in minimal glucose sensing technology, several key milestones must be addressed, the most critical of which involves the efficient encapsulation of GOx and HRP such that the activity of the encapsulated catalytic system is approximately equivalent to that of the catalytic solution in free solution, while operating in a glucose-limited regime. The meeting of this milestone will involve developing techniques to alter substrate diffusion through the polyelectrolyte complex and/or optimize the concentration of immobilized GOx and HRP, which could expedite the use of this technology in sensing applications.

Acknowledgment. The authors acknowledge Michelle Prevot and Dmitry Shchukin for SEM image acquisition. Financial support for this work was provided by the National Institutes of Health (R01EB000739) and by the Sofja Kovelevskaja Program of the Alexander von Humboldt Foundation and the German Ministry of Education and Research.

References and Notes

(1) Clark, H. A.; Kopelman, R.; Tjalkens, R.; Philbert, M. A. *Anal. Chem.* **1999**, *71*, 4837−43.
(2) McShane, M. J. *Diabetes Technol. Ther*. **2002**, *4*, 533−8.
(3) McShane, M. J.; Russell, R. J.; Pishko, M. V.; Cote, G. L. *IEEE Eng. Med. Biol. Mag.* **2000**, *19*, 36−45.
(4) Russell, R. J.; Pishko, M. V.; Gefrides, C. C.; McShane, M. J.; Cote, G. L. *Anal. Chem.* **1999**, *71*, 3126−32.
(5) Santra, S.; Wang, K.; Tapec, R.; Tan, W. *J. Biomed. Opt.* **2001**, *6*, 160−6.
(6) Brasuel, M.; Kopelman, R.; Miller, T. J.; Tjalkens, R.; Philbert, M. A. *Anal. Chem* **2001**, *73*, 2221−8.
(7) Brown, J. Q.; McShane, M. J. *IEEE Eng. Med. Biol. Mag.* **2003**, *22*, 118−123.
(8) Brown, J. Q.; McShane, M. J. *IEEE Sens. J.* **2005**, *5*, 1197−1205.
(9) Chinnayelka, S.; McShane, M. J. *J. Fluoresc.* **2004**, *14*, 585−95.
(10) Guice, K. B.; Caldorera, M. E.; McShane, M. J. *J. Biomed. Opt.* Submitted.
(11) Trau, D.; Renneberg, R. *Biosens. Bioelectron.* **2003**, *18*, 1491−9.
(12) Yu, A.; Caruso, F. *Anal. Chem*. **2003**, *75*, 3031−7.
(13) Wang, Y.; Caruso, F. *Chem. Mater*. **2005**, *17*, 953−961.
(14) Caruso, F.; Schuler, C. *Langmuir* **2000**, *16*, 9595−9603.
(15) Stein, E. W.; McShane, M. J. *IEEE Trans. Nanobiosci.* **2003**, *2*, 133−7.
(16) Brown, J. Q.; Srivastava, R.; McShane, M. J. *Biosens. Bioelectron.* **2005**, *21*, 212−216.
(17) Srivastava, R.; Brown, J. Q.; Zhu, H.; McShane, M. J. *Biotechnol. Bioeng*. **2005**, *91*, 124−31.
(18) Iler, R. K. *J. Colloid Sci.* **1966**, *21*, 569−594.
(19) Antipov, A. A.; Sukhorukov, G. B.; Leporatti, S.; Radtchenko, I. L.; Donath, E.; Mohwald, H. *Colloids Surf., A* **2002**, *198*−*200*, 535−541.
(20) Decher, G.; Hong, J. D. *Makromol. Chem., Macromol. Symp.* **1991**, *46*, 321.
(21) Lvov, Y. *Electrostatic layer-by-layer assembly of proteins and polyions*; Marcel Dekker: New York, 2000.
(22) Lvov, Y.; Caruso, F. *Anal. Chem.* **2001**, *73*, 4212−7.
(23) Sukhorukov, G. B.; Donath, E.; Davis, S.; Lichtenfeld, H.; Caruso, F.; Popov, V. I.; Moehwald, H. *Polym. Adv. Technol.* **1998**, *9*, 759−767.
(24) Antipov, A. A.; Shchukin, D.; Fedutik, Y.; Petrov, A. I.; Sukhorukov, G. B.; Mohwald, H. *Colloids Surf., A* **2003**, *224*, 175−183.
(25) Sukhorukov, G. B.; Shchukin, D. G.; Dong, W.-F.; Mohwald, H.; Lulevich, V. V.; Vinogradova, O. I. *Macromol. Chem. Phys.* **2004**, *205*, 530−535.
(26) Sukhorukov, G. B.; Antipov, A. A.; Voigt, A.; Donath, E.; Möhwald, H. *Macromol. Rapid Commun.* **2001**, *22*, 44−46.
(27) Tiourina, O. P.; Antipov, A. A.; Sukhorukov, G. B.; Larionova, N. I.; Lvov, Y.; Mohwald, H. *Macromol. Biosci.* **2001**, *1*, 209−214.
(28) Shchukin, D. G.; Patel, A. A.; Sukhorukov, G. B.; Lvov, Y. M. *J. Am. Chem. Soc.* **2004**, *126*, 3374−3375.
(29) Volodkin, D. V.; Petrov, A. I.; Prevot, M.; Sukhorukov, G. B. *Langmuir* **2004**, *20*, 3398−3406.
(30) Petrov, A. I.; Volodkin, D. V.; Sukhorukov, G. B. *Biotechnol. Prog.* **2005**, *21*, 918−925.
(31) Volodkin, D. V.; Larionova, N. I.; Sukhorukov, G. B. *Biomacromolecules* **2004**, *5*, 1962−1972.
(32) Wang, Y.; Caruso, F. *Chem. Commun.* **2004**, *13*, 1528−1529.
(33) Yu, A.; Wang, Y.; Barlow, E.; Caruso, F. *Adv. Mater.* **2005**, *17*, 1737−1741.
(34) Dai, J.; Balachandra, A. M.; Ii, J. L.; Bruening, M. L. *Macromolecules* **2002**, *35*, 3164−3170.
(35) Lvov, Y.; Antipov, A. A.; Mamedov, A.; Mohwald, H.; Sukhorukov, G. B. *Nano Lett.* **2001**, *1*, 125−128.
(36) Miller, M. D.; Bruening, M. L. *Langmuir* **2004**, *20*, 11545−11551.
(37) Brown, J. Q.; McShane, M. J. *Biosens. Bioelectron*. In press.
(38) Zhang, K.; Wu, X. Y. *J. Controlled Release* **2002**, *80*, 169−178.
(39) Malikkides, C. O.; Weiland, R. H. **1982**, *24*, 2419−2439.
(40) Jung, D.-Y.; Magda, J. J.; Han, I. S. *Macromolecules* **2000**, *33*, 3332−3336.
(41) Brinkley, M. *Bioconjug. Chem.* **1992**, *3*, 2−13.
(42) Harris, J. J.; Bruening, M. L. *Langmuir* **2000**, *16*, 2006−2013.
(43) Zhu, H.; McShane, M. J. *Langmuir* **2005**, *21*, 424−430.
(44) Shen, F. H.; Feng, Q. L.; Wang, C. M. *J. Cryst. Growth* **2002**, *242*, 239−244.
(45) Balabushevich, N. G.; Tiourina, O. P.; Volodkin, D. V.; Larionova, N. I.; Sukhorukov, G. B. *Biomacromolecules* **2003**, *4*, 1191−1197.
(46) Liu, X.; Bruening, M. L. *Chem. Mater*. **2004**, *16*, 351−357.
(47) Hoshi, T.; Saiki, H.; Kuwazawa, S.; Tsuchiya, C.; Chen, Q.; Anzai, J. I. *Anal. Chem.* **2001**, *73*, 5310−5315.
(48) Ibarz, G.; Dahne, L.; Donath, E.; Mohwald, H. *Chem. Mater*. **2002**, *14*, 4059−4062.
(49) Salloum, D. S.; Schlenoff, J. B. *Biomacromolecules* **2004**, *5*, 1089−1096.
(50) Gergely, C.; Bahi, S.; Szalontai, B.; Flores, H.; Schaaf, P.; Voegel, J.-C.; Cuisinier, F. J. G. *Langmuir* **2004**, *20*, 5575−5582.
(51) Carlsson, F.; Linse, P.; Malmsten, M. *J. Phys. Chem. B* **2001**, *105*, 9040−9049.
(52) Rojas, O. J.; Ernstsson, M.; Neuman, R. D.; Claesson, P. M. *Langmuir* **2002**, *18*, 1604−1612.
(53) Schoeler, B.; Poptoshev, E.; Caruso, F. *Macromolecules* **2003**, *36*, 5258−5264.

BM050304J